16th World Conference on Earthquake, 16WCEE 2017
Santiago Chile, January 9th to 13th 2017
Paper N° 2298
Registration Code: S-C1464682469

EXPERIMENTAL ASSESSMENT OF UNREINFORCED EXTERIOR BEAM-COLUMN JOINTS

M.T. De Risi[(1)], P. Ricci[(2)], G.M. Verderame[(3)], G. Manfredi[(4)]

[(1)] Research Fellow, University of Naples Federico II – Department of Structures for Engineering and Architecture, mariateresa.derisi@unina.it
[(2)] Research Fellow, University of Naples Federico II – Department of Structures for Engineering and Architecture, paolo.ricci@unina.it
[(3)] Associate Professor, University of Naples Federico II – Department of Structures for Engineering and Architecture, verderam@unina.it
[(4)] Full Professor, University of Naples Federico II – Department of Structures for Engineering and Architecture, gamanfre@unina.it

Abstract

Reinforced Concrete (RC) buildings designed according to obsolete seismic codes or for gravity loads only are widespread in Italian and Mediterranean building stock. In seismic performance assessment of these typical non-conforming buildings, collapse safety might be significantly affected by non-linear behavior of joints that are involved in the failure mechanism, especially if they are characterized by poor structural detailing, such as the lack of an adequate transverse reinforcement in the joint panel.

Few reliable approaches for modeling all sources of nonlinearity are proposed in literature for poorly designed beam-column joints because of relatively poor information from experimental tests. Even if a quite significant amount of research on seismic performance of unreinforced joints has been carried out in last years, a very few portion of them handled with specimens with plain hook-ended longitudinal bars. A small number of experimental results include also the analysis of local aspects, such as the evaluation of joint shear strain. Therefore, a higher number of tests is necessary to deeper understand joint seismic response in order to validate the existing models or calibrate new ones.

The current study aims at improving the understanding of seismic performance of exterior joints without transverse reinforcement in non-conforming RC buildings through experimental tests. Four full-scale exterior unreinforced beam-column joint sub-assemblages are tested under cyclic loading. The specimens are different for beam longitudinal reinforcement ratio and for typology of longitudinal bars (plain or deformed). Two different kinds of joint failure are expected, with or without the yielding of the adjacent beam. Strain gauges located on beam bars and displacement transducers on the joint panel allow the complete definition of both the main deformability contributions, namely fixed-end-rotation and shear strain of joint panel, highlighting the difference between the observed failure modes. Design criteria, adopted setup and experimental results are described and discussed.

From the analysis of the global experimental responses, it is observed that the higher the beam longitudinal reinforcement ratio, the higher the joint shear strength, and that the post-peak degrading behavior is always controlled by the response of the joint panel. The analysis of local responses highlighted that the sum of the main deformability contributions due to joints (joint panel shear strain and rotation at beam/joint interface) represents the major part of the imposed drift for all tests. In particular, in tests for which the beam reaches the yielding moment, the contribution of the deformation mechanism associated to the rotation at beam-joint interface is predominant, particularly in the case of plain longitudinal reinforcement.

Keywords: exterior non-conforming RC joints; experimental assessment; plain versus deformed bars

1. Introduction

Beam-column joints without transverse reinforcement represent one of the main sources of seismic vulnerability in non-ductile Reinforced Concrete (RC) buildings. Several research studies have been carried out aimed at investigating the behavior of unreinforced beam-column joints under seismic action, with numerical or experimental-based approaches.

Experimental campaigns have mainly studied the behavior of exterior unreinforced joints (for instance [1]-[9]), mainly due to their higher seismic vulnerability compared to interior joints [10]. Most of these experimental studies have been focused on joint shear strength, evaluating the influence of different geometrical or mechanical parameters on this strength. Fewer studies focused on the different deformation mechanisms due to the joint [9], their contribution to the overall deformability of the sub-assemblage (i.e., to frame deformability) [8], and to the total energy dissipation capacity [11]. Furthermore, there is a quite small number of studies focused on the local shear response of the joint panel ([1], [2], [7]).

Different researchers have collected experimental databases of tests on unreinforced exterior joints ([12], [13], [14]) in order to propose and validate analytical or empirical capacity models, mainly aimed at providing the joint shear strength. However, despite a relatively large amount of experimental data, there is still a great inhomogeneity (e.g. for anchorage details or presence of slab) in the typologies of tests presented in literature. For instance, there is a very limited amount of data on joints built with plain longitudinal bars ([15], [16], [17]), compared with the available data on joints with deformed bars.

The present study aims at contributing to the investigation of seismic performance of unreinforced exterior joints in non-ductile RC buildings through experimental tests, analyzing the shear strength and the local stress-strain behavior of the joint panel. To this aim, four full-scale exterior unreinforced joint sub-assemblages different for longitudinal reinforcement – plain or deformed – and design typology – for gravity loads only or in compliance with an obsolete seismic code – are tested under cyclic loading. The specimens are intended to be representative of two typical design practices in force in Italy between 1960s and 1990s. Two distinct failure modes are expected, depending on the beam longitudinal reinforcement ratio obtained from design, namely a joint shear failure prior to beam yielding (hereinafter referred to as J failure mode) or following beam yielding (hereinafter referred to as BJ failure mode). The global and local experimental responses are presented and discussed in next Sections.

2. Experimental program and setup

2.1 Design and detailing of specimens

Geometry and longitudinal reinforcement amount in beams and columns are defined by means of a simulated design procedure [18] according to code prescriptions and design practices in force in Italy between 1960s and 1990s. The specimens named Test #1D and Test #1P are related to a frame designed according to seismic prescriptions (for high seismicity level), in compliance with the Italian codes D.M. 1975 [19], D.M. 1981 [20], D.M. 1992 [21]. The specimens named Test #2D and Test #2P are related to a frame designed for gravity loads only. Column axial load corresponding to gravity loads acting on these joints is equal to 260 kN. Test #1D and #2D are characterized by deformed bars, whereas Test #1P and #2P are reinforced with plain bars.

The four tests are identical for geometry. Beam rectangular sectional area is 50 cm high (h_b=50cm) and 30 cm depth (b_b=30 cm). Columns have a square sectional area with height (h_c) equal to 30 cm. Column length was designed to be representative of typical interstorey height (3.40 m), and column shear length (L_c) is equal to 1.45 m; the beam length (up to the centerline of the column) is equal to 1.80 m, and its shear length is (L_b) is equal to 1.65m (see Fig. 1). Beam longitudinal reinforcement ($A_{s,b}$) is defined on the basis of flexural demand obtained from the simulated design. Minimum amount of longitudinal reinforcement required in columns are slightly modified with respect to the simulated design and a weak beam-strong column hierarchy is obtained. As shown in Fig. 1, beams and columns are always symmetrically reinforced. According to ASCE-SEI/41 [10]

prescriptions two failure modes are expected (see also [22] and [23]): a J-failure mode for Test #1D and Test #1P, and a BJ-failure mode for Test #2D and Test #2P.

For Test #1P and #2P (with plain bars), top and bottom beam longitudinal bars are anchored with end hooks bent inside the joint core: the internal curvature radius of hooks is equal to 3 times the bar diameter (according to the Italian constructive practice in force until 70's), namely equal to 60 mm for Test #1P and 42 mm for Test #2P. For Test #1D and #2D (with deformed bars), top and bottom beam longitudinal bars are hooked bent at 90° into the joint core for a length of 20 cm.

Transverse reinforcement in beams and columns was designed to avoid shear failure, in order to not preclude joint shear failure; no transverse reinforcement was located in the joint panel zone, in compliance with code prescriptions in force in the reference time assumed for the design.

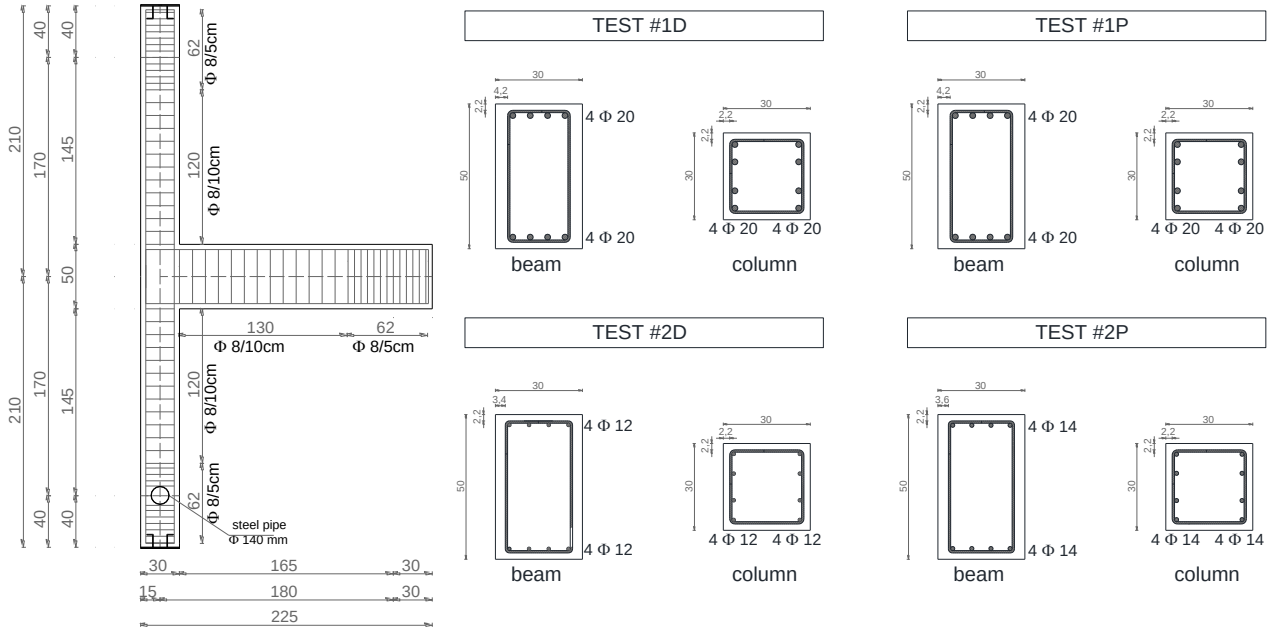

Fig. 1 - Geometry and reinforcement details

2.2 Materials properties

Concrete compressive strength for all specimens was evaluated on four cubic samples (CSs) of the casted concrete. Values of 28-day cylindrical strength for each CS and their mean value are reported in Table 1.

Table 1 - Material properties

Steel properties				Concrete properties	
Diameter [mm]	**Yield strength (f_y) [MPa]**	**Ultimate strength (f_t) [MPa]**	**Hardening ratio (f_t/f_y) [-]**	**Cubic sample**	**Cylindrical compressive strength (f_c) [MPa]**
20 D	487	596	1.22	CS1	27.2
12 D	459	560	1.22	CS2	29.2
8 D	492	607	1.23	CS3	31.2
20 P	344	465	1.35	CS4	27.4
14 P	316	489	1.55	mean	28.8

Commercial typology of the adopted reinforcing steel is B450C, for deformed (D) bars. Steel typology B450C shows mechanical properties that can be assimilated to FeB44k typology, widespread in Italy between 1970s and 1990s. Mechanical properties of the reinforcing steel for plain (P) longitudinal reinforcement are

similar to AQ42 commercial typology (adopted in Italy until '60s) or FeB22k (employed since '70s). Table 1 shows mean values of their mechanical properties (yield strength, f_y; ultimate strength, f_t; and hardening ratio, f_t/f_y).

2.3 Test setup, monitoring and loading scheme

A schematic of the loading apparatus is shown in Fig. 2. The column was mounted horizontally with pinned supports at both ends and the specimen was constrained to the strong floor by means of two rigid steel frames. Steel spherical hinges were placed between the beam end and the floor to limit friction and to allow tip beam free movement. The axial load (N) was applied in load control, using a hydraulic jack and transferred to the column through four pre-stressed rods connected to strong steel plates, located on the top and bottom of the column. In particular, a constant value of axial load equal to N=260kN (corresponding to an axial load ratio equal to ν=0.10) was applied. A hydraulic actuator applied the lateral load in displacement control at the end of the beam by means of a loading collar.

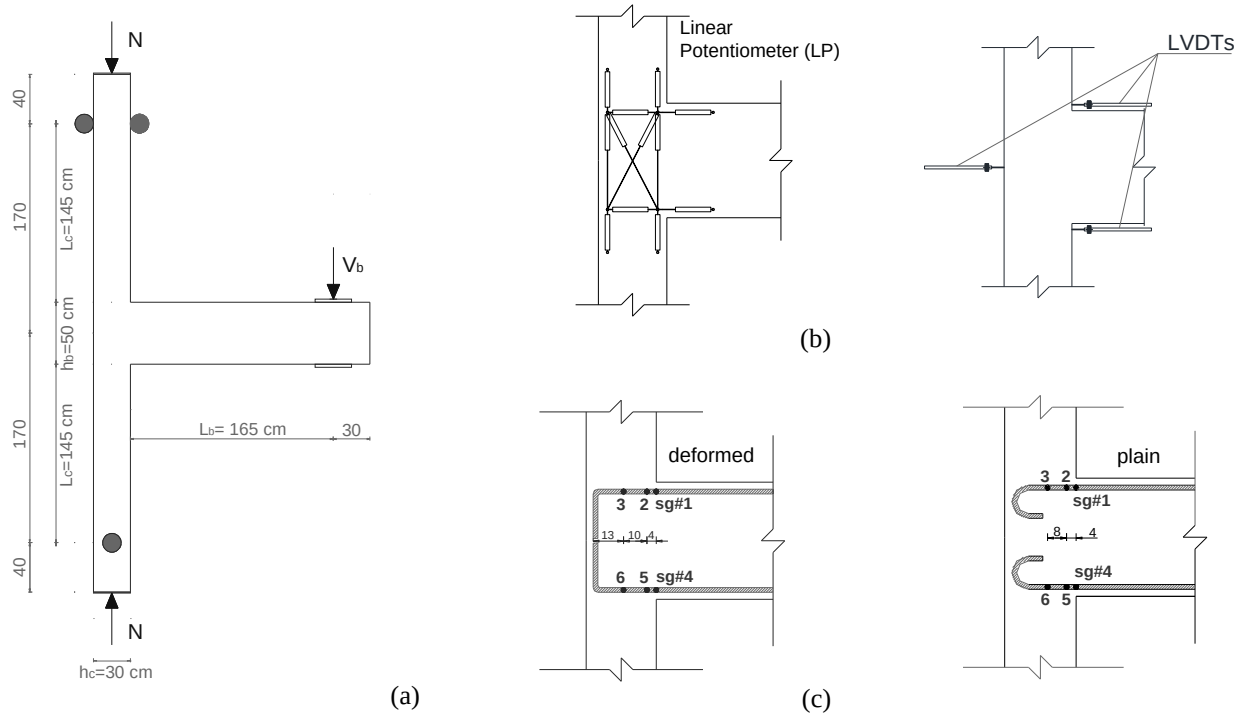

Fig. 2 -Test setup (a), joint panel instrumentation (b) and strain gauges location (c)

Twelve Linear Potentiometer sensors (LPs) adopted to measure joint shear strain and beam(column)-joint interface rotations were located in the joint panel along longitudinal reinforcement layers of beams and columns and along the diagonals of the joint panels, as shown in Fig. 2b. A wire potentiometer was placed at the end of the beam to measure beam deflection. Strains in beam longitudinal reinforcement were measured, too, by means of six strain gauges (sgs) located as shown in Fig. 2c (three on a bar in the top layer and three on a bar in the bottom layer). Two additional Linear Variable Displacement Transducers (LVDTs) located along beam depth (Fig. 2b) were used in Test #2D in order to have a more reliable measure of beam(column)-joint interface rotation contribution.

The loading procedure consisted of displacement-controlled steps beginning at a 0.25% drift followed by steps of 0.50%, 0.75%, 1.00%, 1.50%, 2.00%, 3.00%, 4.00% and 6.00% drift. Each drift step consisted of 3 cycles of push and pull. The term drift represents the ratio between the imposed displacement at beam tip (Δ_b) and beam length (from the loaded end to the column centerline), namely, drift is equal to $\Delta_b/(L_b+h_c/2)$.

3. Global force-drift response

In this Section, lateral load-displacement response of the specimens is analyzed, and the evolution of observed damage with increasing imposed displacement is briefly described. More details about the evolution of damage in the specimens can be found in [22] and [23].

3.1 Joints with deformed bars

The results in terms of beam lateral load versus drift response related to Test #1D are reported in Fig. 3a, where experimental response appears quite symmetric during the push-pull cycles. The initial stiffness showed a first reduction at beam-joint interface cracking, for a beam load of 37 kN (predicted value for beam cracking was equal to 28 kN). Then a more significant stiffness reduction is observed when the applied drift ranges between 0.50% and 0.75%, when first joint panel cracking occurred, first in negative loading direction, at -60 kN beam load, and then in positive direction, for a beam load value of +54 kN. Peak load was reached for a drift equal to +1.40% for positive loading direction and -1.38% for negative loading direction. Peak values of beam lateral load were +74.0 kN and -72.4 kN, for positive and negative loading direction, respectively. Since beam yielding was expected to occur for a beam lateral load value of 155.6 kN, such a test can be classified as J-failure, i.e. joint shear failure occurring before yielding of the beam. Such a classification was confirmed by the measures of bar strains provided by the strain gauges located at beam-joint interface, which measured a maximum value of 1.37‰, namely lower than 2.43‰ (corresponding to yielding). The post-peak phase, controlled by joint failure, is characterized by a gradual degradation with a softening stiffness (calculated on the envelope of first cycles) equal to about -4% of the initial uncracked stiffness. When the test was interrupted (first cycle at 6.00% drift), the strength reduction was equal to 47% and 53% of the peak load, in positive and negative direction, respectively.

The results in terms of beam lateral load versus drift response related to Test #2D are reported in Fig. 3b. Also in this case, experimental response appears quite symmetric during the push-pull cycles. The initial stiffness showed a significant reduction when the applied drift ranges between 0.25% and 0.50%, when first cracks along beam-joint interface started to occur (associated with a localized strength reduction), corresponding to a beam load equal to 29 kN (quite close to the predicted value for beam cracking, i.e. 23 kN). Then, joint cracking occurs, first in negative loading direction, at -54 kN beam load, and then in positive direction, for a beam load value of +49 kN. Peak load was reached for a drift equal to 0.88% for positive loading direction and -0.69% for negative loading direction. The corresponding peak values of beam lateral load were +58.3 kN and -54.0 kN, respectively. Since beam yielding was expected to occur for a beam lateral load value of 52.9 kN, such a test can be classified as BJ-failure, i.e. joint shear failure occurring after yielding of beam. Such a classification was confirmed by the measures of bar strains provided by the strain gauges located at beam-joint interface, which measured a maximum value of 2.88‰, namely higher than 2.30‰ (corresponding to yielding). At the same time, the peak load is lower than beam flexural strength (65.5 kN), for both loading directions, confirming that peak strength is limited by the achievement of joint shear failure. The post-peak phase, controlled by joint failure, is characterized by a gradual degradation with a softening stiffness (calculated on the envelope of first cycles) equal to about -6% of the initial uncracked stiffness. When the test was interrupted (third cycle at 2.00% drift), the strength reduction was equal to 49% and 56% with respect to the peak load, respectively in positive and negative directions. The strength reduction, evaluated at the first cycle at 2.00% drift, was equal to 26% and 31% of the peak load, respectively in positive and negative directions.

3.2 Joints with plain bars

The response in terms of beam lateral load versus drift is reported in Fig. 3c for Test #1P; experimental response is quite symmetric during the push-pull cycles. The initial stiffness showed a first reduction at beam-joint interface cracking, corresponding to a beam load equal to 43 kN (predicted value for beam cracking was equal to 26kN); then, a more significant reduction of stiffness occurs when the applied drift ranges between 0.50% and 0.75%, together with the first joint panel cracking, first in negative loading direction, at -53 kN beam load, and then in positive direction, for a beam load value of 60 kN. Peak load was reached for a drift equal to 1.44% for positive loading direction and -1.43% for negative loading direction. Peak values of beam lateral load were +79.2 kN and -74.8 kN, for positive and negative loading direction respectively. Since beam yielding was

expected to occur for a beam lateral load equal to 109.4 kN, such a test, similarly to Test #1D, can be classified as J-failure. Such a classification was confirmed by the measures of bar strains provided by the strain gauges located at beam-joint interface, which measured a maximum value of 0.95‰, namely lower than 1.72‰ (corresponding to yielding). The post-peak phase, controlled by joint failure, is characterized by a gradual degradation with a softening stiffness (calculated on the envelope of first cycles) equal to about -7% of the initial uncracked stiffness. When the test was interrupted (at the end of the first cycle at 6.00% drift), the strength reduction (calculated on the envelope of first cycles) was equal to 45% and 50%, in positive and negative direction, respectively.

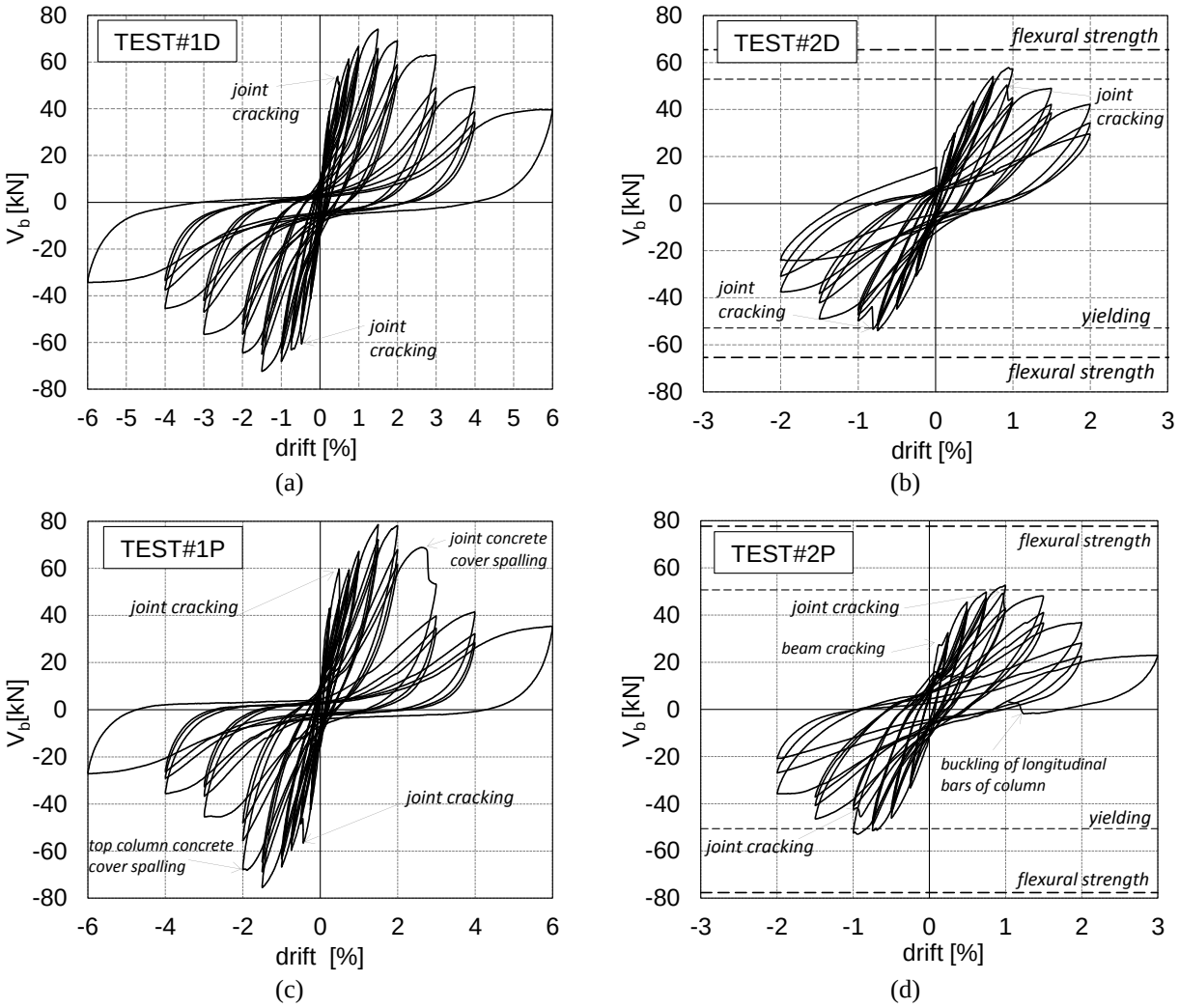

Fig. 3 -Beam lateral load versus drift: cyclic response

Beam lateral load versus drift response related to Test #2P is reported in Fig. 3d, where the experimental response appears symmetric during the push-pull cycles. The initial stiffness showed a significant reduction when the applied drift ranges between 0.25% and 0.50%, when first cracks along beam-joint interface started to occur, corresponding to a beam load equal to 28 kN, quite close to the predicted value for beam cracking, i.e. 23kN. Joint cracking occurs first in positive loading direction, at 49 kN beam load, and then in negative direction, for a beam load value of -45 kN. Peak load was reached for a drift equal to 0.95% for positive loading direction, and -0.89% for negative loading direction. Peak values of beam lateral load were 52.8 kN and -52.6 kN, for positive and negative loading direction, respectively. Since beam yielding was expected to occur for a beam lateral load value of 50.6 kN, this test can be classified as BJ-failure, as confirmed by strain gauges measures. Such a classification was confirmed by the measures of bar strains provided by the strain gauges located at beam-joint interface, which measured a maximum value of 6.85‰, namely lower than 1.58‰

(corresponding to yielding). At the same time, the peak load is lower than beam flexural strength (77.6 kN), for both loading directions, confirming that peak strength is limited by the achievement of joint shear failure. The post-peak phase, controlled by joint failure, is characterized by a gradual degradation with a softening stiffness (calculated on the envelope of first cycles) equal to about -6% of the initial uncracked stiffness. When the test was interrupted, the strength reduction (calculated on the envelope of first cycles) was equal to 68% and 44%, in positive and negative directions respectively.

Final damage state for all tests is reported in Fig. 4.

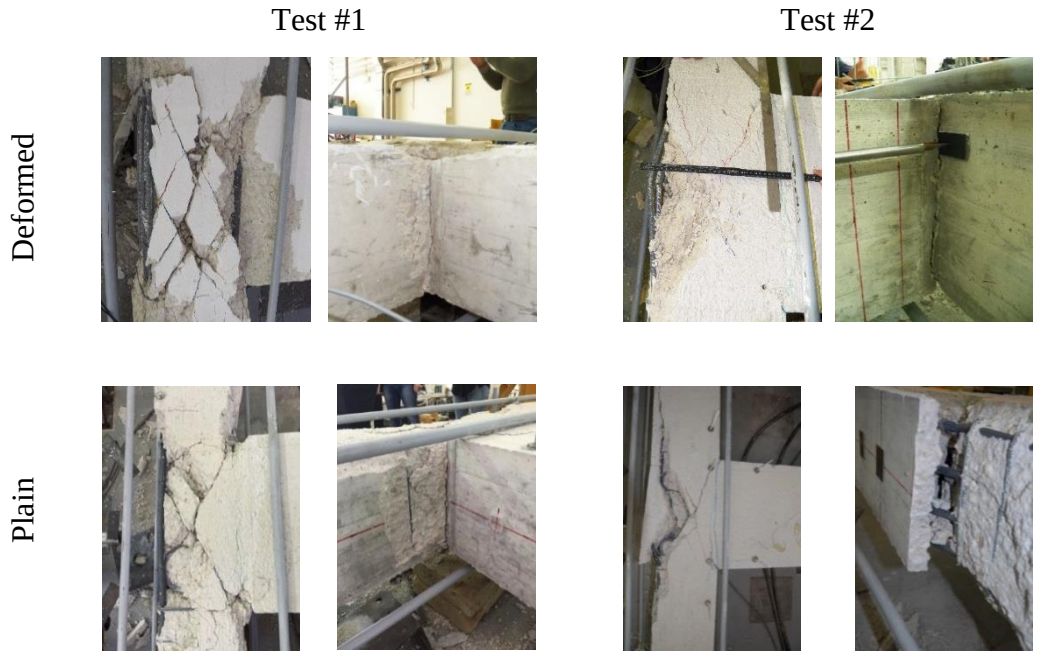

Fig. 4 – Damage state at the end of tests

4. Local behavior

4.1 joint shear response

Linear potentiometers located on the joint panel are employed to calculate joint shear strain, as suggested and adopted by previous experimental works (e.g. [24], [25], [22], [23]), according to which joint shear strain can be expressed as shown in Eq. (1):

$$\gamma_{joint,i} = \frac{\varepsilon_\theta - \varepsilon_x \cos^2\theta - \varepsilon_y \sin^2\theta}{\sin\theta\cos\theta} \quad (1)$$

where, ($\gamma_{joint,i}$) is the joint shear strain obtained using a certain set of strain measures, ε_x and ε_y are strains in the horizontal and vertical directions, respectively, and ε_θ is the strain in the diagonal direction with an angle of θ measured from the horizontal axis. Four estimates of the joint shear strain were obtained by four triangles of LPs located in the joint panel (see Fig. 2b) by using Eq. (1). Joint shear strain (γ_{joint}) was calculated as the mean of these four estimates. Joint shear is calculated on the base of equilibrium equations. In particular, joint shear demand V_{jh} is obtained depending on the beam load V_b, according to Eq. (2) (see also Fig. 2a for notation):

$$V_{jh} = \frac{V_b \cdot L_b}{d^*} - \frac{V_b \cdot (L_b + h_c/2)}{(2L_c + h_b)} \quad (2)$$

where L_b is the beam clear length, (L_b+h_c/2) is the total length of the beam, ($2L_c$+h_b) represents the total length of bottom and top columns; d^* the internal lever arm of beam section, evaluated as $d^* = (\beta \cdot d)$, where d is the

effective depth while β is assumed equal to 0.90. Joint shear stress (τ_j) can be calculated as the ratio between joint shear (V_{jh}) and joint horizontal area (A_{jh}).

In Fig. 5, experimental responses in terms of $\tau_j/\sqrt{f_c}$ versus γ_{joint} are reported for all tests. Data are represented until LPs measures are considered reliable, i.e. until cracks significantly involved the support points of LPs. Moreover, Fig. 5 also shows the envelope $\tau_j/\sqrt{f_c}$ versus γ_{joint} at the end of the first cycle of each imposed drift value, for all tests. Table 2 shows the values of $\tau_j/\sqrt{f_c}$ corresponding to first shear cracking ($\tau_{j,cr}/\sqrt{f_c}$) and peak strength ($\tau_{j,max}/\sqrt{f_c}$) of the joint panel. It can be observed that Test #2 (D and P) exhibited a lower $\tau_{j,max}/\sqrt{f_c}$ respect to the corresponding Test #1 (D and P).

Table 2 - Experimental values of $\tau_j/\sqrt{f_c}$ corresponding to shear cracking and peak strength of joint panel

Test #	$V_{b,cr}$ [kN]	$V_{b,max}$ [kN]	L_b [mm]	L_b-h_c/2 [mm]	$2L_c$ [mm]	$\tau_{j,cr}/\sqrt{f_c}$ [$\sqrt{MPa}$]	$\tau_{j,max}/\sqrt{f_c}$ [$\sqrt{MPa}$]	$\tau_{j,y}/\sqrt{f_c}$ [$\sqrt{MPa}$]	$\tau_{j,flex}/\sqrt{f_c}$ [$\sqrt{MPa}$]
1D	60.0	74.0	1800	1650	3400	0.43	0.53	1.11	-
2D	54.0	58.3	1800	1650	3400	0.38	0.41	0.38	0.46
1P	59.7	79.2	1800	1650	3400	0.43	0.57	0.72	-
2P	49.0	52.8	1800	1650	3400	0.35	0.38	0.39	0.56

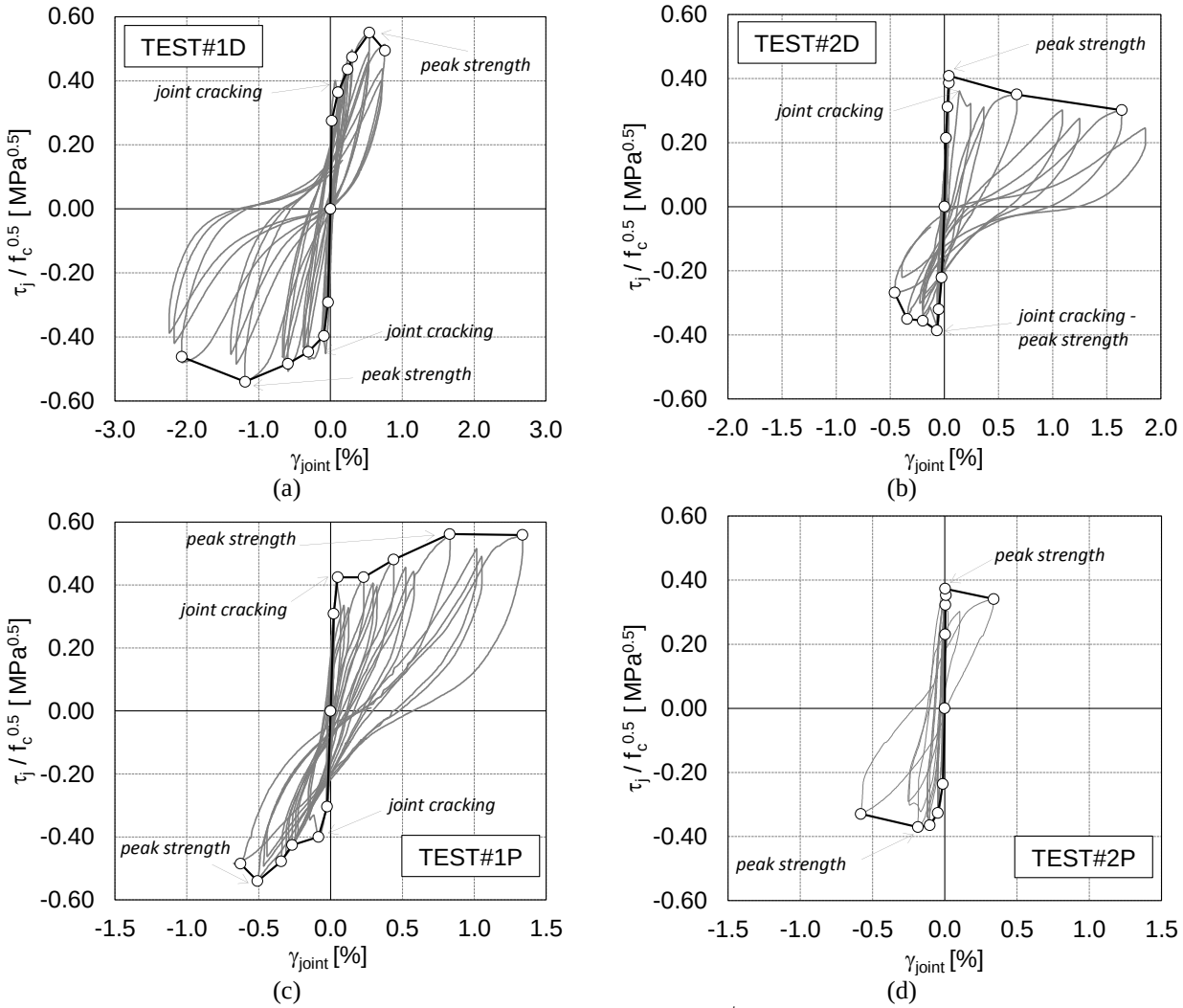

Fig. 5 - Joint panel response in term of shear stress $\tau_j/\sqrt{f_c}$ – shear strain γ_j relationship

4.2 Rotation at beam/columns-joint interface

The rotation at the beam(column)-joint interface – θ_{sb} (θ_{sc}) – and, thereby, its contribution to the overall deformability – can be estimated through LPs located along longitudinal bars of column at the interface with joint panel (Fig. 2b). Note that such a rotation does not correspond to "fixed-end-rotation" since LPs provide the measure of the whole crack width at the interface, including the slippage of longitudinal bars both from the panel zone and from the element. Fig. 6 shows the rotation θ_s as a function of the imposed drift for all the tests, evaluated for beam, top column and bottom column. Experimental data are plotted until the support points of the corresponding LPs were affected by significant cracks, as explained previously. The rotation (θ_s) is evaluated at the end of the first sub-cycle for each drift value and generally appears quite symmetric in positive and negative directions.

It can be observed that θ_s is generally lower for the columns than for the beam, and, for each drift level, $\theta_{s,b}$ is generally higher for Tests #1P and #2P (with plain pars), with respect to Tests #1D and #2D (with deformed bars), respectively, as expected because of the difference in reinforcement typology. The higher values of $\theta_{s,b}$ in the case of BJ-failure (Test #2D and #2P) compared with J-failure (Test #1D and #1P) are clearly shown. Finally, for all tests, the rotation at beam/joint interface increases with increasing drift also in post-peak phase, i.e. with decreasing shear in beam.

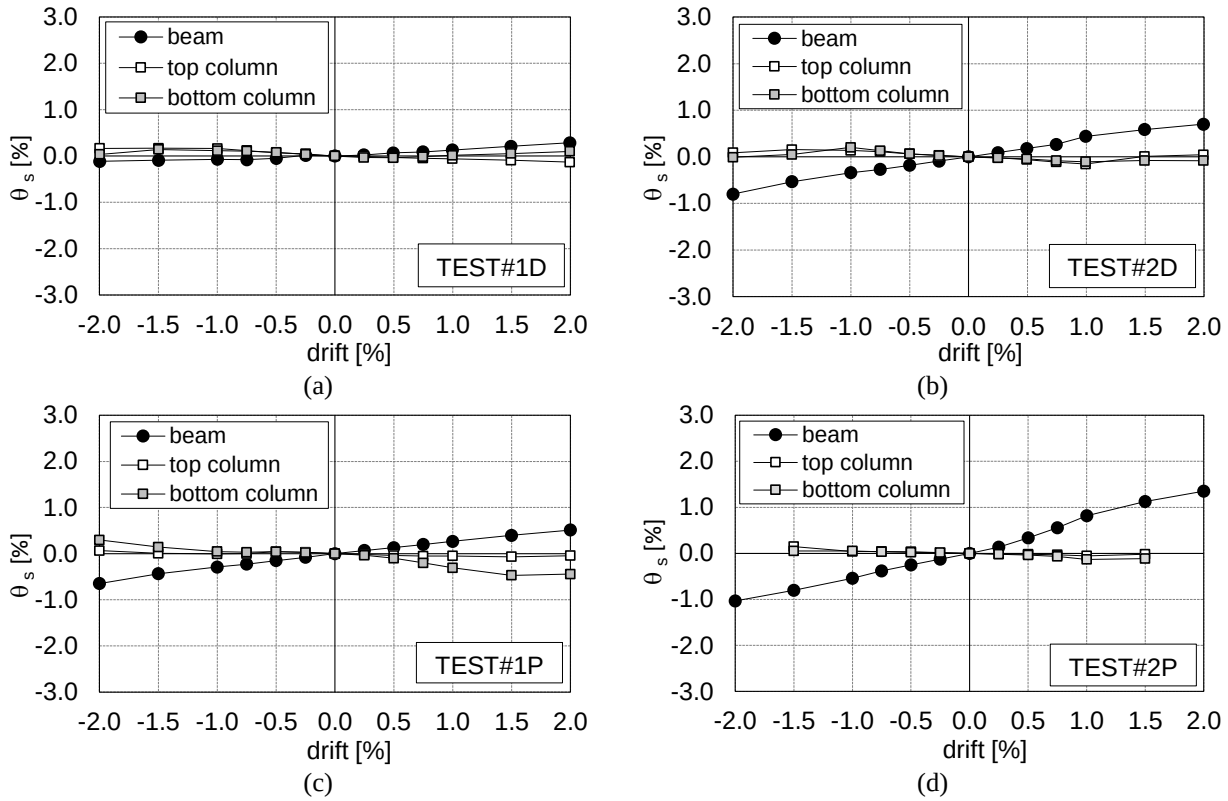

Fig. 6 - Rotation θ_s related to beam, top column and bottom column

4.3 Analysis of deformability contributions

In this Section, the contributions due to joint to the overall deformability of the sub-assemblage are evaluated by analyzing the relationship between the quantities γ_{joint}, $\theta_{s,b}$ and $\theta_{s,c}$ - calculated at the end of the first sub-cycle for each imposed drift level, as previously - with the imposed drift. Beam top displacement Δ_b due to each of the analyzed quantities is calculated on the basis of equations of rotational equilibrium of rigid body by respecting the constraint conditions, as shown in Eq.s (3) (see also Fig. 2a for notation):

$$\Delta_b^{\gamma_{joint}} = \gamma_{joint} \cdot L_b - (\gamma_{joint} \cdot h_b)\frac{(L_b + 0.5h_c)}{(2L_c + h_b)}$$

$$\Delta_b^{\theta_{s,b}} = \theta_{s,b} \cdot L_b \tag{3}$$

$$\Delta_b^{\theta_{s,c}} = (\theta_{s,c}^{top} + \theta_{s,c}^{bot}) \cdot L_c \cdot \frac{(L_b + 0.5h_c)}{(2L_c + h_b)}$$

where $\theta_{s,c}^{top}$ and $\theta_{s,c}^{bot}$ represent the rotation θ_s for top and bottom columns, respectively.

By dividing Δ_b due to γ_{joint}, $\theta_{s,b}$ and $\theta_{s,c}$ for the beam length L_b, the drift contribution to the global deformability is obtained for each component. Such contributions are shown in Fig. 7, averaged between positive and negative loading directions, as a function of the total imposed drift (until LPs measures are reliable and for the first cycle at each drift level). For all specimens, it can be observed that the sum of deformability contributions due to joint shear strain and rotation at beam-joint interface ($\theta_{joint} = \gamma_{joint} + \theta_{s,b}$) represents the majority of the imposed drift.

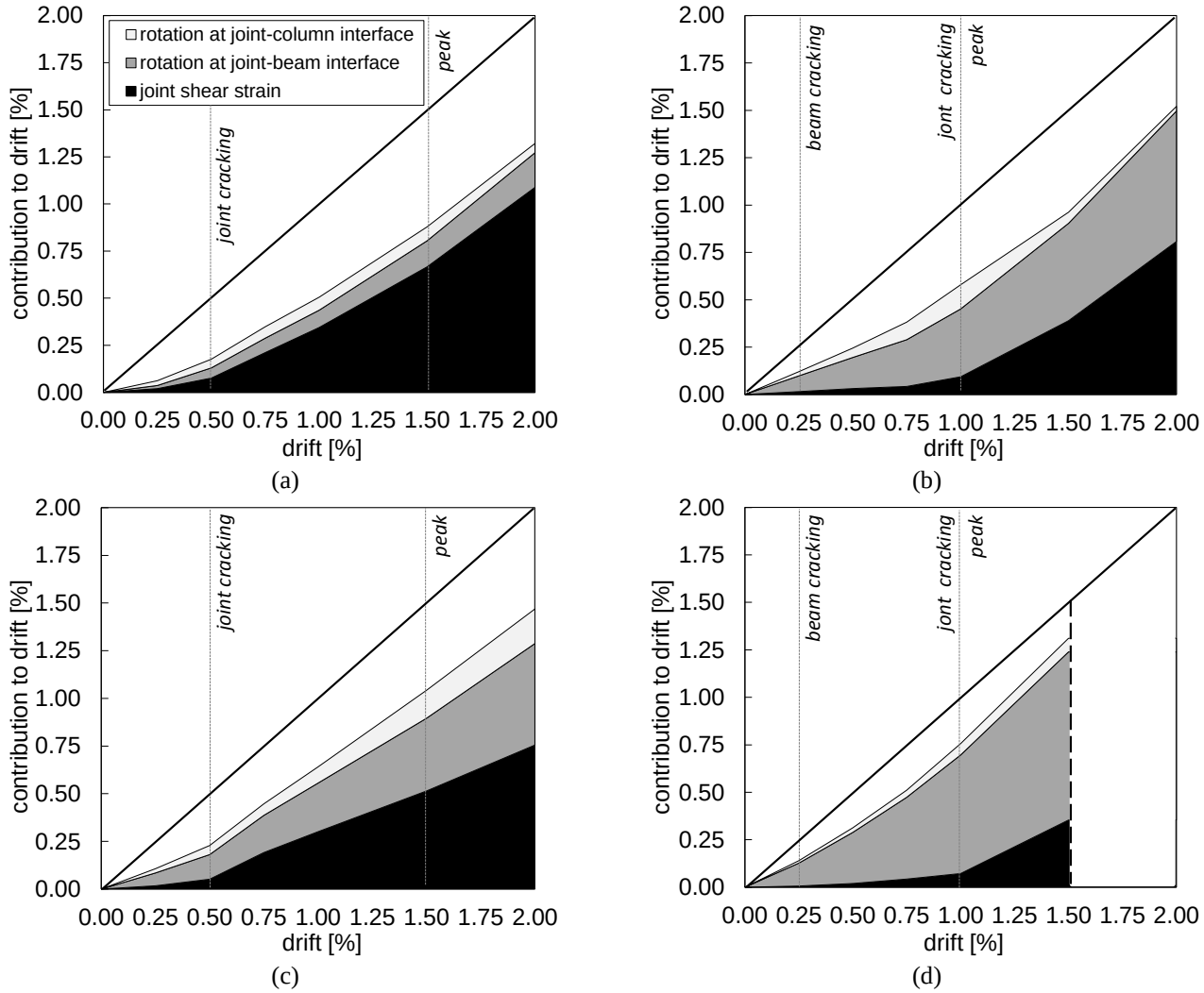

Fig. 7 - Contributions to the overall imposed drift: Test #1D (a), #2D (b), #1P (c), and #2P(d)

For Test #1D (Fig. 7a) – which exhibited a J-failure mode – θ_{joint} reaches a maximum of about 50% of the imposed drift at the peak point (drift=1.50%) and about the 60% at 2.00% drift. For Test #2D (Fig. 7b) – which

exhibited a BJ-failure mode – θ_{joint} reaches a maximum value of about 70% at 2.00% drift. Similarly to Test #1D, for Test #1P (Fig. 7c) – which exhibited a J-failure mode – θ_{joint} reaches a maximum of about 50% of the overall imposed drift at the peak point (drift=1.50%) and about the 60% at 2.00% drift. For Test #2P (Fig. 7d) (BJ-failure mode) the maximum value of θ_{joint} is about 80% (at 1.50% drift) of the overall imposed drift.

In particular, when J-failure occurred (Tests#1D and #1P), the shear deformability contribution due to joint panel (γ_{joint}) is systematically predominant with respect to the contribution due to rotation at the beam/joint interface ($\theta_{s,b}$) - after cracking of joint panel occurred - as expected. However, fixed the imposed drift level, rotation at beam-joint interface is higher in Test#1P (plain bars) than in Test #1D, as expected. Vice-versa, in tests characterized by BJ-failure mode (Tests#2D and #2P), $\theta_{s,b}$ is generally predominant with respect to the contribution due to joint shear deformability. However, right after joint cracking, the contribution of γ_{joint} rapidly increases, while $\theta_{s,b}$ is almost constant, despite yielding of longitudinal reinforcement. Also in this case, fixed the imposed drift level, rotation at beam/joint interface is higher in Test#2P (plain bars) than in Test #2D, as expected.

Furthermore, the contributions to the dissipated hysteretic energy reflect the influence of each deformation mechanism (joint shear strain, rotations at beam(column)-joint interface) to the total deformability of the sub-assemblages just pointed out. In tests characterized by a J-failure mode (Tests #1D and #1P) the contribution to the dissipated energy due to joint shear strain is generally the highest one; on the contrary, in tests characterized by a BJ-failure mode (Tests #2D and #2P) the contribution to the dissipated energy due to beam-joint interface rotation is predominant [25].

Finally, note that the contribution that misses to reach 100% of the imposed drift in Fig. 7 is due to shear and flexural deformability of beam and columns, and progressively reduces its percentage weight for increasing drift levels.

5. Conclusions

In the present work, experimental results of four tests on unreinforced exterior RC beam-column joints were shown and analyzed. The joint specimens were designed according to code prescriptions and design practices in force in Italy between 1960s and 1990s, for gravity loads only or according to old seismic prescriptions. Depending on the different beam longitudinal reinforcement ratio, two distinct failure modes were expected, namely joint shear failure without beam yielding and joint shear failure following beam yielding.

Experimental results, in terms of lateral load-displacement response, showed that:

- in Tests #1D and #1P, with a higher beam mechanical longitudinal reinforcement ratio, the attainment of maximum strength is controlled by joint failure, without flexural yielding of the beam (J-failure mode);
- in Tests #2D and #2P, with a lower beam mechanical longitudinal reinforcement ratio, the attainment of maximum strength is controlled by joint failure and follows the flexural yielding of the beam (BJ-failure mode); actually, peak load is higher than the expected flexural yielding and lower than the expected flexural strength of the beam.

The post-peak degrading behavior was always controlled by the response of the joint panel. Note that the higher the beam longitudinal reinforcement ratio, the higher the joint shear strength, confirming proposals from literature according to which joint shear strength decreases as ductility demand in beam increases.

The analysis of local responses highlighted that the sum of the main deformability contributions due to joints (joint panel shear strain and rotation at beam/joint interface) represents the major part of the imposed drift for all tests. In particular:

- in Tests #1D and #1P (J-failure mode), after the cracking of the joint panel, the joint shear strain contribution is systematically predominant with respect to the contribution due to rotation at the beam(column)-joint interface;

- in Tests #2D and #2P (BJ-failure mode), the rotation at beam/joint interface contribution is systematically predominant until cracking of the joint panel occurs; vice-versa, after joint cracking, the contribution of joint shear strain rapidly increases, while the rotation at beam/joint interface is almost constant, despite yielding of longitudinal reinforcement.

Moreover, in specimens with plain bars the rotation at beam-joint interface was higher than in the corresponding specimens with deformed bars, as expected. Finally, in tests characterized by a BJ-failure mode (Tests #2D and #2P), the contribution of the deformation mechanism associated to the rotation at beam-joint interface was predominant, particularly in the case of plain longitudinal reinforcement.

6. Acknowledgements

This work was developed under the financial support of ReLUIS-DPC 2014-2018 PR 2- Linea Strutture in cemento armato, funded by the Italian Department of Civil Protection (DPC). This support is gratefully acknowledged.

7. References

[1] Clyde C, Pantelides CP, Reaveley LD (2000). Performance-Based Evaluation of Exterior Reinforced Concrete Buildings Joints for Seismic Excitation, PEER Report, No. 2000/05, Pacific Earthquake Engineering Research Center, University of California, Berkeley, USA.

[2] Pantelides CP, Hansen J, Nadauld J, Reaveley LD (2002). Assessment of Reinforced Concrete Building Exterior Joints with Substandard Details, PEER Report, No. 2002/18, Pacific Earthquake Engineering Research Center, University of California, Berkeley, USA.

[3] Tsonos A.G. and Papanikolaou K.V. (2003). Post-Earthquake Repair and Strengthening of Reinforced Concrete Beam-Column Connections (Theoretical & Experimental Investigation). Bulletin-New Zealand society for earthquake engineering 36.2: 73-93.

[4] Antonopoulos C.P. and Triantafillou T.C. (2003). Experimental investigation of FRP-strengthened RC beam-column joints. Journal of composites for construction, 7 (1): 39-49.

[5] Wong H. F. (2005) Shear strength and seismic performance of non-seismically designed RC beam–column joints. Ph.D. thesis. Hong Kong University of Science and Technology.

[6] Del Vecchio C, Di Ludovico M, Balsamo A, Prota A, Manfredi G, Dolce M. Experimental investigation of exterior RC beam–column joints retrofitted with FRP systems. J Compos Constr 2014;18(4):04014002.

[7] Genesio G. (2012). Seismic assessment of RC exterior beam-column joints and retrofit with haunches using post-installed anchors. Ph.D. thesis, University of Stuttgart, Germany.

[8] Masi A., Santarsiero G., and Nigro D. (2013). Cyclic tests on external RC beam-column joints: role of seismic design level and axial load value on the ultimate capacity. Journal of Earthquake Engineering 17.1, 2013: 110-136.

[9] Park S. and Mosalam K.M. (2013). Simulation of Reinforced Concrete Frames with Nonductile Beam-Column Joints, Earthquake Spectra, 29(1), 233-257.

[10] ASCE/SEI 41, Seismic rehabilitation of existing buildings. American Society of Civil Engineers, Reston, VA, USA, 2007.

[11] Melo, J., Varum, H., and Rossetto, T. (2014). Cyclic behaviour of interior beam–column joints reinforced with plain bars. Earthquake Engineering and Structural Dynamics.

[12] Park S and Mosalam KM. (2012). Analytical model for predicting the shear strength of unreinforced exterior beam-column joints, ACI Structural Journal 109, 149–159.

[13] Jeon J.-S. (2013). Aftershock vulnerability assessment of damaged reinforced concrete buildings in California. Ph.D. thesis, School of Civil and Environmental Engineering, Georgia Institute of Technology, GA.

[14] De Risi M.T. (2015). Seismic performance assessment of RC buildings accounting for structural and non-structural elements. Ph.D. Thesis, University of Naples Federico II, Naples, Italy.

[15] Pampanin S., Calvi G.M., and Moratti M. (2002). Seismic behavior of RC beam-column joints designed for gravity only. 12th European Conference on Earthquake Engineering, paper n.726, London 2002.

[16] Chen T. H. (2006). Retrofit strategy of non-seismically designed frame systems based on a metallic haunch system.

[17] Melo J., Varum H., Rossetto T., and Costa A. (2012). Cyclic response of RC beam-column joints reinforced with plain bars: An experimental testing campaign. In Proceedings of the 15 th World Conference on Earthquake Engineering. Lisbon, Portugal (pp. 24-28).

[18] Verderame G.M., Polese M., Mariniello C., Manfredi G. (2010). A simulated design procedure for the assessment of seismic capacity of existing reinforced concrete buildings, Adv Eng Softw 41(2):323–335.

[19] Decreto Ministeriale n. 40 del 3/3/1975. Approvazione delle norme tecniche per le costruzioni in zone sismiche. G.U. n. 93 dell'8/4/1975. (in Italian)

[20] Decreto Ministeriale del 7/3/1981. Dichiarazione di zone sismiche nelle regioni Basilicata, Campania e Puglia. (in Italian)

[21] Decreto Ministeriale del 14/02/1992. Norme tecniche per il calcolo, l'esecuzione ed il collaudo delle strutture in cemento armato, normale e precompresso e per le strutture metalliche. (in Italian)

[22] De Risi M.T., Ricci P., Verderame G.M., Manfredi G. (2016). Experimental assessment of unreinforced exterior beam-column joints with deformed bars. Engineering Structures (DOI:10.1016/j.engstruct.2016.01.016).

[23] Ricci P., De Risi M.T., Verderame G.M., Manfredi G. (2016). Experimental tests of unreinforced exterior beam-column joints with plain bars. Engineering Structures (DOI: 10.1016/j.engstruct.2016.03.033).

[24] Engindeniz M. (2008). Repair and Strengthening of Pre-1970 Reinforced Concrete Corner Beam-Column Joints Using CFRP Composites, PhD Thesis, Civil and Environmental Engineering Department, Georgia Institute of Technology, August 2008.

[25] Hassan W.M. (2011). Analytical and Experimental Assessment of Seismic Vulnerability of Beam-Column Joints without Transverse Reinforcement in Concrete Buildings, PhD Dissertation, University of California, Berkeley, California, USA.

[26] Verderame G.M., De Risi M.T., Ricci P., (2016). Experimental investigation of unreinforced exterior beam-column joints with plain and deformed bars. Journal of Earthquake Engineering (doi: 10.1080/13632469.2016.1233917).